Central European Journal of Energetic Materials, **2014**, *11*(3), 433-442
ISSN 2353-1843

Preparation and Characterization of HMX/Estane Nanocomposites

Xiaofeng SHI, Jingyu WANG*, Xiaodong LI, Chongwei AN

Chemical Industry and Ecology Institute, North University of China, Taiyuan Shanxi, 030051, P. R. China
**E-mail: profound_000@163.com; xiaofeng_shi1987@163.com*

Abstract: A new insensitive explosive based on octahydro-1,3,5,7-tetranitro-1,3,5,7-tetrazocine (HMX) was prepared by spray drying using Estane 5703 as a binder. Scanning electron microscopy was used to characterize the morphology and particle size of the HMX/Estane 5703 nanocomposites. The composites were analyzed by X-ray diffractometry and differential scanning calorimetry and their impact sensitivity was determined. For comparison, raw HMX was also tested using these three methods. The nanocomposite morphology was found to be microspherical (1 to 8 μm diameter) and composed of many tiny particles, 30 to 150 nm in size. The crystal type of the HMX/Estane 5703 nanocomposites was unchanged. The activation energy, self-ignition temperature and average drop height of the raw HMX were 515.66 kJ·mol^{-1}, 278.63 °C and 18.4 cm, respectively. In comparison, the corresponding values for the HMX/Estane 5703 nanocomposites were 488.92 kJ·mol^{-1}, 279.3 °C and 75.4 cm, respectively.

Keywords: HMX, Estane 5703, spray drying, nanocomposites, thermal stability

1 Introduction

Although high explosives (HEs) have attracted much attention because of their higher energy, they cannot be used directly in weapons because of their sensitivity. Various binders have therefore been added to HEs to reduce their sensitivity [1-5]. A number of studies have been conducted on Estane (a polyurethane) as one of the favorite binders [6-12]. Plastic bonded explosives (PBXs) coated with Estane display many advantages, such as excellent toughness and waterproofness. However, the required binder ratio in PBXs is usually 5 to 10% [13-15], which reduces the HE energy. An alternative way to reduce the sensitivity of HEs has been

studied, namely, by changing their crystal size and morphology. Micro- and nanometer-sized HEs have been prepared by various techniques [16-18]. These HEs retain their energy but are less sensitive. Spherical and cubic explosive particles have been prepared to reduce the HE sensitivity [19-21]. Many researchers have shown that nanometer-sized spherical explosive particles, which are coated with a small amount of binder, can be prepared in a single-step, spray drying process [22-24]. This technology not only reduces the HE sensitivity, but also reduces the HE energy loss. The spray drying process has many advantages, such as accurate control of the process conditions and rapid preparation. For example, raw octahydro-1,3,5,7-tetranitro-1,3,5,7-tetrazocine (HMX) and HMX/polyvinyl acetate have been prepared by a spray drying process [25]. However, insufficient research has been conducted into spray drying and additional experimentation is required. In the present work, HMX-based nanocomposites with Estane 5703 as the binder were prepared by spray drying. Furthermore, the nanocomposite properties were characterized and analyzed in detail.

2 Experimental Part

2.1 Materials

HMX was produced by Gansu YingGuang Chemical Industry Group Co., Ltd.; Estane 5703 was provided from Dongguan XiangLin Plastic Co., Ltd.; acetone was purchased from Tianjin TianDa Chemicals Co., Ltd.

2.2 Preparation of HMX-based nanocomposites

To begin with, both HMX (3 g) and Estane 5703 (0.0928 g) were dissolved together in acetone at 40 °C at a concentration of 3 wt% by sonication. The co-solution was then spray-dried to produce nanoparticles using a Mini Buchi 290 spray dryer. The flow rate of the feed solution and the cyclone was set to 50 $mL \cdot min^{-1}$ and 36 $m^3 \cdot h^{-1}$, respectively. The temperature of the dry inlet gas (N_2) was kept at 65 °C. Finally, the products were collected in an electrically grounded, glass collection vessel.

2.3 Characterization

The morphology and size of the HMX-based nanocomposites were studied using a Hitachi S-4800 scanning electron microscope (SEM) (Hitachi Ltd., Japan). The accelerating voltage was 1.0 kV. A DX-2700 diffractometer (Dandong Haoyuan Instrument Co., Ltd., China) was used to compare the crystal types of the raw HMX and the HMX/Estane nanocomposites by X-ray diffractometry (XRD). The testing

conditions were: tube voltage 40 kV; tube current 30 mA; stepping angle 0.03° and sample interval 0.5 s. The crystal size of the HMX-based nanocomposites was also estimated using the Scherrer equation. Differential scanning calorimetry (DSC) experiments were conducted in an N_2 atmosphere using a Setaram DSC131 instrument (Setaram Instrumentation Co., France) and aluminum crucibles with a hole in the cap. The test conditions were: sample mass 0.7 mg; N_2 flow rate 15 mL·min^{-1} and sample heating rates 20, 10 and 5 K·min^{-1}. The impact sensitivity of the HMX-based nanocomposites was tested at room temperature using an ERL type 12 drop hammer apparatus with a sample mass of 35 ± 1 mg and a drop weight of 5 ± 0.002 kg. Four groups of samples and 25 of the same sample from each group were tested. The results were obtained in terms of the critical drop-height of 50% explosion probability (H_{50}) and the standard deviation (S).

3 Results and Discussion

3.1 SEM characterization

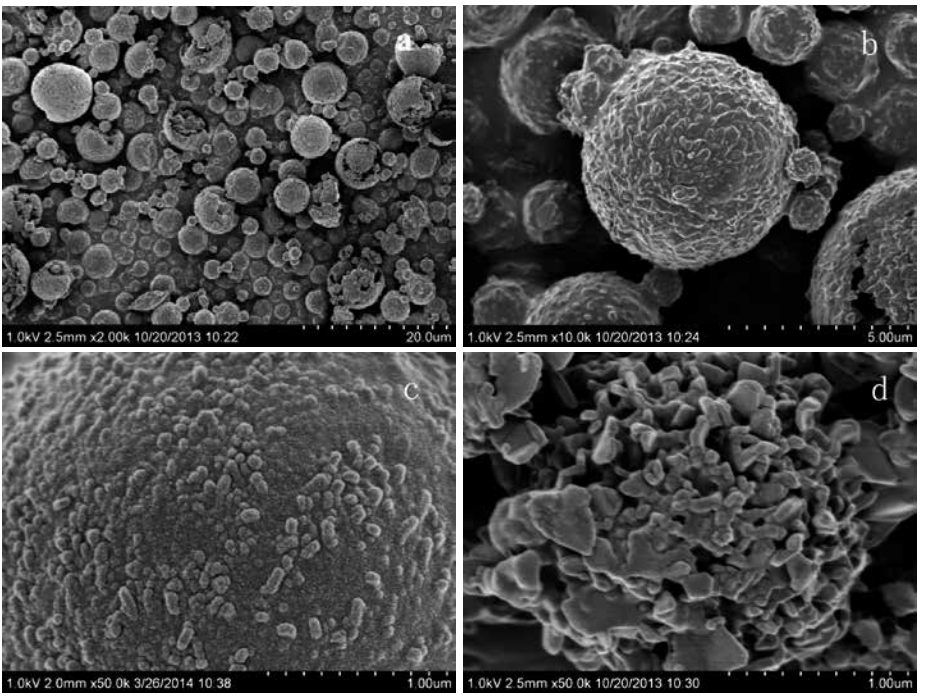

Figure 1. SEM images of HMX-based nanocomposites at different magnifications.

Figure 1 shows SEM micrographs of the HMX-based nanocomposites. Figure 1(a) shows that the sample particle size range from 1 to 8 μm. The samples are microspherical, with rough surfaces and are composed of many tiny particles (see Figure 1(b)) that stick together (see Figure 1(c) and (d)). Most of the particles are spherical and clavate and are 30 to 150 nm in size.

3.2 XRD characterization

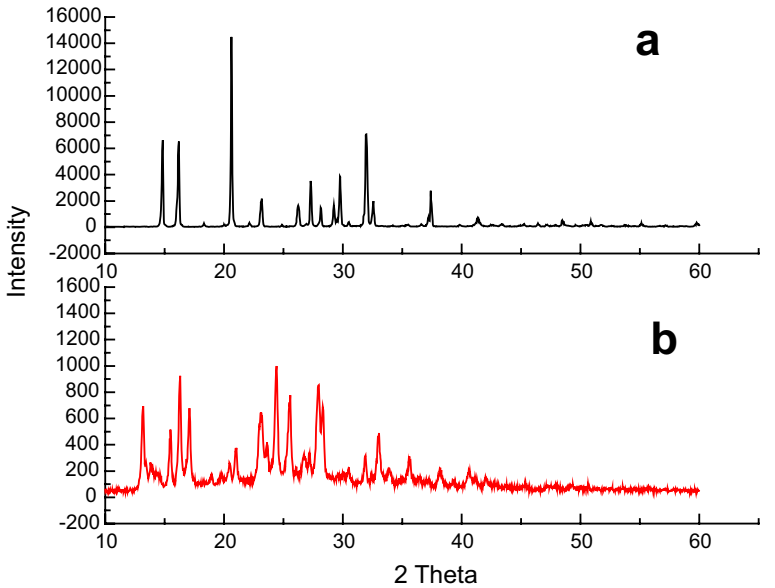

Figure 2. X-ray diffraction patterns of raw HMX (a) and HMX-based nanocomposites (b).

As is shown in Figure 2, compared with raw HMX, the HMX-based nanocomposites have similar diffraction angles but more unidentifiable diffraction peaks because of the addition of Estane 5703. Moreover, the diffraction peaks of the HMX-based nanocomposites are wider and weaker (diffraction peak intensity below 1000 a.u.) than those of raw HMX (diffraction peak intensity of ~2000-16000 a.u.). This is because the diffraction peaks of the sample weaken and disappear as the sample particle size is reduced to the nano-level. MID Jade 9.0 software was used to fit the diffraction peaks of the HMX/Estane 5703 sample and to calculate the full width at half maximum (FWHM) of its diffraction pattern. The average crystallite size of the HMX/Estane 5703 sample was estimated using the Scherrer equation (Equation 1) [26].

$$D = \frac{K\lambda}{B\cos\theta} \tag{1}$$

D is the particle length in nm; K is the Scherrer constant, 0.89; λ is the wavelength of the X-ray, 0.154 nm; B is the full width at half maximum (FWHM) of the diffraction pattern in radians; θ is the diffraction angle in radians.

Three different diffraction angles (2θ) and the FWHM of the major characteristic diffraction peaks were collected from 10-45°. The diffraction angles and FWHM were 16.297, 24.428, 33.036° and 0.199, 0.236, 0.272°, respectively. The results show that the HMX crystal sizes were 39.8, 34.0 and 30.1 nm, which is consistent with the SEM micrographs.

3.3 Thermal decomposition characteristics

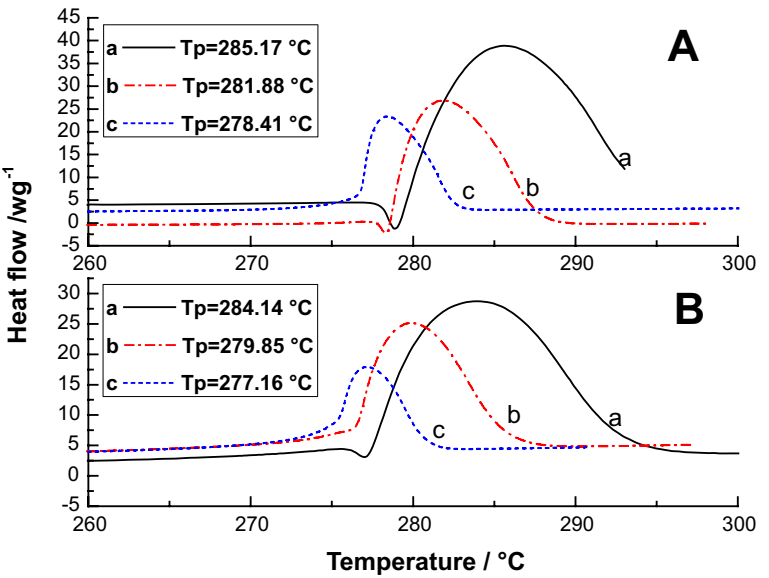

Figure 3. DSC curves of raw HMX (A) and HMX-based nanocomposites (B) at heating rates of 20 K·min^{-1} (a), 10 K·min^{-1} (b), and 5 K·min^{-1} (c).

Figure 3 shows the DSC curves of raw HMX and the HMX-based nanocomposites at 5, 10 and 20 K·min^{-1} heating rates. In Figure 3(A), the exothermic peak temperatures of raw HMX were 285.17, 281.88 and 278.41 °C at heating rates of 20, 10 and 5 K·min^{-1}, respectively. Similarly, Figure 3(B) indicates that the exothermic peak temperatures of the HMX-based nanocomposites were 284.14, 279.85 and 277.16 °C at heating rates of 20, 10

and 5 K·min^{-1}, respectively. A comparison between these two images shows that the exothermic peak temperatures of the HMX-based nanocomposites differ little from those of raw HMX. This proves that HMX and Estane 5703 are compatible. The thermal decomposition kinetics parameters of raw HMX and the HMX-based nanocomposites can be calculated by the Kissinger method (Equation 2) [27].

$$\ln\frac{\beta_i}{T_{pi}^2} = \ln\frac{AR}{E} - \frac{E}{RT_{pi}} \tag{2}$$

β_i is the heating rate in K·min^{-1}; T_{pi} is the temperature, in K, of the exothermic peak at heating rate β_i; E is the activation energy in J·mol^{-1}; A is the pre-exponential factor; R is the gas constant, 8.314 J·mol^{-1}·K^{-1}.

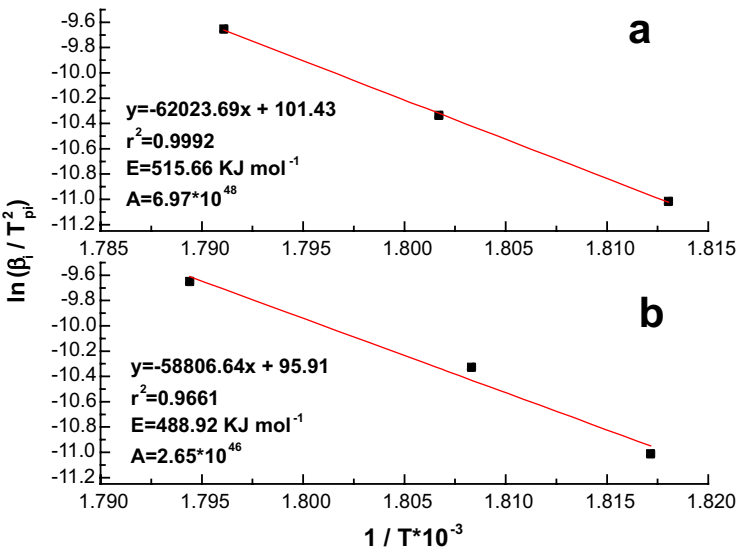

Figure 4. Kissinger plots of raw HMX (a) and HMX-based nanocomposites (b).

As is shown in Figure 4, a straight line is obtained when the values of $\ln(\beta_i/T_{pi}^2)$ are plotted against $1/T_{pi}$. The activation energy can be calculated from the slope (–E/R). The pre-exponential factor can be calculated from the intercept [ln(AR/E)]. The results are presented in Figures 4 (a) and (b), which show that the activation energy of the HMX-based nanocomposites is decreased only slightly from that of raw HMX.

3.4 Thermal Stability

Thermal stability refers to the high temperature-resistance property of materials and their ability to maintain stable properties with heating. It can be expressed using the self-ignition temperature (T_b), which can be estimated from Equations 3 [28] and 4 [29].

$$T_e = T_{pi} - b\beta_i - c\beta_i^2 \tag{3}$$

$$T_b = \frac{E - \sqrt{E^2 - 4RET_e}}{2R} \tag{4}$$

where β_i is the heating rate in K·min^{-1}; T_e is the peak temperature, in K, when β_i is zero; T_{pi} is the peak temperature, in K, of decomposition at β_i; b and c are constants; T_b is the self-ignition temperature in K; E is the activation energy in J·mol^{-1}; R is the universal gas constant, 8.314 J·mol^{-1}·K^{-1}.

For raw HMX, T_e and T_b were calculated to be 273.72 and 278.63 °C, respectively. In comparison, T_e and T_b of the HMX-based nanocomposites were calculated to be 274.11 and 279.3 °C, respectively. The thermal stability of the HMX-based nanocomposites is therefore slightly better than that of raw HMX.

3.5 Impact sensitivity

Table 1. Impact sensitivity of raw HMX and HMX-based nanocomposites

Sample	Impact sensitivity H_{50} [cm]				
	Experiment				Average
	1 (S)	2 (S)	3 (S)	4 (S)	
Raw HMX	17.5 (0.09)	19.8 (0.06)	17.8 (0.05)	18.5 (0.06)	18.4
HMX/Estane 5703	75.5 (0.07)	78.7 (0.07)	71.3 (0.06)	75.9 (0.05)	75.4

From Table 1, it can be seen that the drop height of the HMX/Estane 5703 nanocomposite is much higher than that of raw HMX from four replicate experiments. This occurs because the Estane 5703 can serve as a diverter or shock absorber under intense impact. The HMX/Estane 5703 nanocomposite have excellent insensitivity.

4 Conclusions

A nanocomposite, which contained HMX and Estane 5703, was prepared successfully by spray drying. The nanocomposites were 1 to 8 μm spheres, composed of spherical, 30-150 nm-sized clavate particles. The crystal type of HMX/Estane 5703 and raw HMX was consistent. The activation energy of HMX/Estane 5703 is slightly lower than that of raw HMX, thereby proving that the energy of the HMX/Estane 5703 is maintained at a high level. Meanwhile, the thermal stability of HMX/Estane 5703 is better than that of raw HMX because of its higher self-ignition temperature. The impact sensitivity of the HMX/Estane 5703 is lower than that of the raw HMX because it has a higher drop height. These combined properties suggest that the HMX/Estane 5703 nanocomposite is an insensitive and high-energy explosive with great potential.

Acknowledgements
We thank the China North Chemical Industries Group Co., Ltd. for support and the Youth Science and Technology Innovation Fund Project Group for the experiments.

5 References

[1] Elbeih A., Zeman S., Pachman J., Effect of Polar Plasticizers on the Characteristics of Selected Cyclic Nitramines, *Cent. Eur. J. Energ. Mater.*, **2013**, *10*(3), 339-349.
[2] Kaur J., Arya V.P., Kaur G., Lata P., Evaluation of the Thermo-mechanical and Explosive Properties of Bimodal and Hybrid Polymer Bonded Explosive (PBX) Compositions Based on HNS and HMX, *Cent. Eur. J. Energ. Mater.*, **2013**, *10*(3), 371-391.
[3] Elbeih A., Zeman S., Jungova M., Akstein Z., Effect of Different Polymeric Matrices on the Sensitivity and Performance of Interesting Cyclic Nitramines, *Cent. Eur. J. Energ. Mater.*, **2012**, *9*(2), 131-138.
[4] Elbeih A., Pachman J., Zeman S., Vávra P., Trzciński W.A., Akštein Z., Detonation Characteristics of Plastic Explosives Based on Attractive Nitramines with Polyisobutylene and Poly(Methyl Methacrylate) Binders, *J. Energ. Mater.*, **2012**, *30*(4), 358-371.
[5] Burnham A.K., Weese R.K., Kinetics of Thermal Degradation of Explosive Binders Viton A, Estane, and Kel-F, *Thermochim. Acta.*, **2005**, *426*(1-2), 85-92.
[6] Barua A., Horie Y., Zhou M., Energy Localization in HMX-Estane Polymer-bonded Explosives during Impact Loading, *J. Appl. Phys.*, **2012**, *111*(5), 054902-054902-11.
[7] Yang L., Surface Polarity of Beta-HMX Crystal and the Related Adhesive Forces with Estane Binder, *Langmuir*, **2008**, *24*(23), 13477-13482.

[8] Barua A., Zhou M., Computational Analysis of Temperature Rises in Microstructures of HMX-Estane PBXs, *Comput. Mech.*, **2013**, *52*(1), 151-159.
[9] Singh G., Prem F.S., Soni P., Studies on Energetic Compounds. Part 28: Thermolysis of HMX and Its Plastic Bonded Explosives Containing Estane, *Thermochim. Acta*, **2003**, *399*(1), 153-165.
[10] Xiao J.J., Huang H., Li J.S., Zhang H., Zhu W., Xiao H.M., Computation of Interface Interactions and Mechanical Properties of HMX-based PBX with Estane 5703 from Atomic Simulation, *J. Mater. Sci.*, **2008**, *43*(17), 5685-5691.
[11] Kim H., Lagutcheva A., Dlott D.D., Surface and Interface Spectroscopy of High Explosives and Binders: HMX and Estane, *Propellants Explos. Pyrotech.*, **2006**, *31*(2), 116-123.
[12] Barua A., Horie Y., Zhou M., Microstructural Level Response of HMX-Estane Polymer-bonded Explosive Under Effects of Transient Stress Waves, *Proc. Roy. Soc. Lond. Math. Phys. Sci.*, **2012**, *468*, (2147), 3725-3744.
[13] Hobbs M.L., Kaneshige M.J., Ignition Experiments and Models of a Plastic Bonded Explosive (PBX 9502), *J. Chem. Phys.*, **2014**, *140*(12), 124203.
[14] Tarver C.M., Modeling Detonation Experiments on Triaminotrinitrobenzene (TATB)-based Explosives LX-17, PBX 9502, and Ultrafine TATB, *J. Energ. Mater.*, **2012**, *30*(3), 220-251.
[15] Wemhoff A.P., Howard W.M., Burnham A.K., Nichols A.L., An LX-10 Kinetic Model Calibrated Using Simulations of Multiple Small-scale Thermal Safety Tests, *J. Phys. Chem. A*, **2008**, *112*(38), 9005-9011.
[16] Wang Y., Jiang W., Song X.L., Deng G.D., Li F.S., Insensitive HMX (Octahydro-1,3,5,7-tetranitro-1,3,5,7-tetrazocine) Nanocrystals Fabricated by High-yield, Low-cost Mechanical Milling, *Cent. Eur. J. Energ. Mater.*, **2013**, *10*(2), 277-287.
[17] Zohari N., Keshavarz M.H., Seyedsadjadi S.A., The Advantages and Shortcomings of Using Nano-sized Energetic Materials, *Cent. Eur. J. Energ. Mater.*, **2013**, *10*(1), 135-147.
[18] Akkbarzade H., Parsafar G.A., Bayat Y. Structural Stability of Nano-sized Crystals of HMX: a Molecular Dynamics Simulation Study, *Appl. Surf. Sci.*, **2012**, *258*(7), 2226-2230.
[19] Song X.L., Wang Y., An C.W., Guo X.D., Dependence of Particle Morphology and Size on the Mechanical Sensitivity and Thermal Stability of Octahydro-1,3,5,7-tetranitro-1,3,5,7-tetrazocine, *J. Hazard. Mater.*, **2008**, *159*(2-3), 222-229.
[20] Kim J.W., Shin M.S., Kim J.K., Kim H.S., Koo K.K., Evaporation Crystallization of RDX by Ultrasonic Spray, *Ind. Eng. Chem. Res.*, **2011**, *50*(21), 12186-12193.
[21] Vijayalakshmi R., Radhakrishnan S., Rajendra P.S., Girish G.M., Arun S.K., Particle Size Management Studies on Spherical 3-Nitro-1,2,4-triazol-5-one, *Part. Syst. Char.*, **2012**, *28*(3-4), 57-63.
[22] Zhigach A.N., Leipunskii I.O., Berezkina N.G., Pshechenkov P.A., Zotova P.A., Kudrov B.V., Gogulya M.F., Brazhnikov M.A., Kuskov M.L., Aluminized Nitramine-based Nanocomposites: Manufacturing Technique and Structure Study, *Combust. Explos. Shock Waves (Engl. Transl.)*, **2009**, *45*(6), 666-677.

[23] Qiu H., Stepanov V., Di Stasio A.R., Chou T.M., Lee W.Y., RDX-based Nanocomposite Microparticles for Significantly Reduced Shock Sensitivity, *J. Hazard. Mater.*, **2011**, *185*(1), 489-493.
[24] An C.W., Li H.Q., Geng X.H., Li J.L., Wang J.Y., Preparation and Properties of 2,6-Diamino-3,5-dinitropyrazine-1-oxide based Nanocomposites, *Propellants Explos. Pyrotech.*, **2013**, *38*(2), 172-175.
[25] Qiu H., Stepanov V., Chou T., Surapaneni A., Di Stasio A.R., Lee W.Y., Single-step Production and Formulation of HMX Nanocrystals, *Powder Technol.*, **2012**, *226*, 235-238.
[26] Shen J.P., Duan X.H., Luo Q.P., Zhou Y., Bao Q.L., Ma Y.J., Pei C.H., Preparation and Characterization of a Novel Cocrystal Explosive, *Cryst. Growth Des.*, **2011**, *11*(5), 1759-1765.
[27] Kissinger H.E., Reaction Kinetics in Differential Thermal Analysis, *Anal. Chem.*, **1957**, *29*(11), 1702-1706.
[28] Zhang T.L., Hu R.Z., Xie Y., Li F.P., The Estimation of Critical Temperatures of Thermal Explosion for Energetic Materials Using Non-isothermal DSC, *Thermochim. Acta.*, **1994**, *244*, 171-176.
[29] Sovizi M.R., Hajimirsadeghi S.S., Naderizadeh B., Effect of Particle Size on Thermal Decomposition of Nitrocellulose, *J. Hazard. Mater.*, **2009**, *168*(2-3), 1134-1139.